Electronic Supplementary Material (ESI) for CrystEngComm.

Supporting Information for:

Structures and photophysical performances of (fluoro)salicylate stabilized polyoxo-titanium clusters

Bang-Chang Zhu,[a] Wei-Hui Fang,*[a] Perumal Emayavaramban,[a] Lei Zhang,*[a] and Jian Zhang[a]

[a]*State Key Laboratory of Structural Chemistry, Fujian Institute of Research on the Structure of Matter, Chinese Academy of Sciences, Fuzhou, Fujian 350002, China.*

Corresponding Author
*E-mail: fwh@fjirsm.ac.cn; LZhang@fjirsm.ac.cn

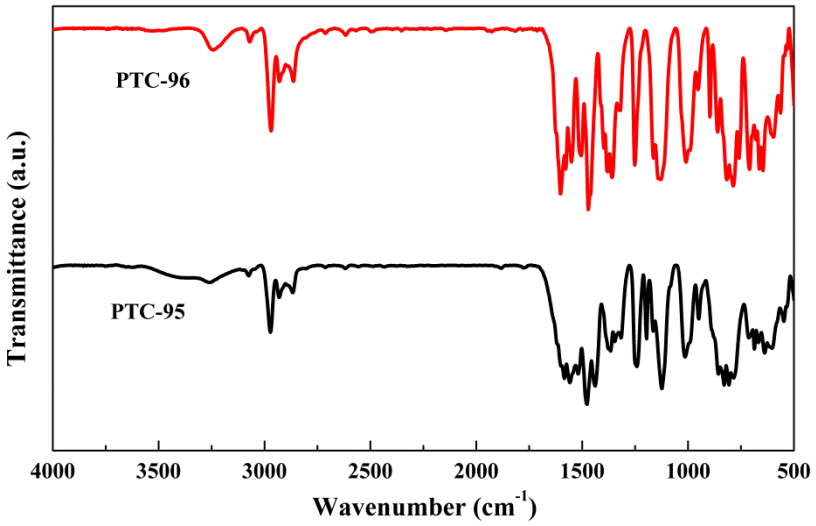

Fig. S1. FT-IR spectra for compounds **PTC-95** and **PTC-96**.

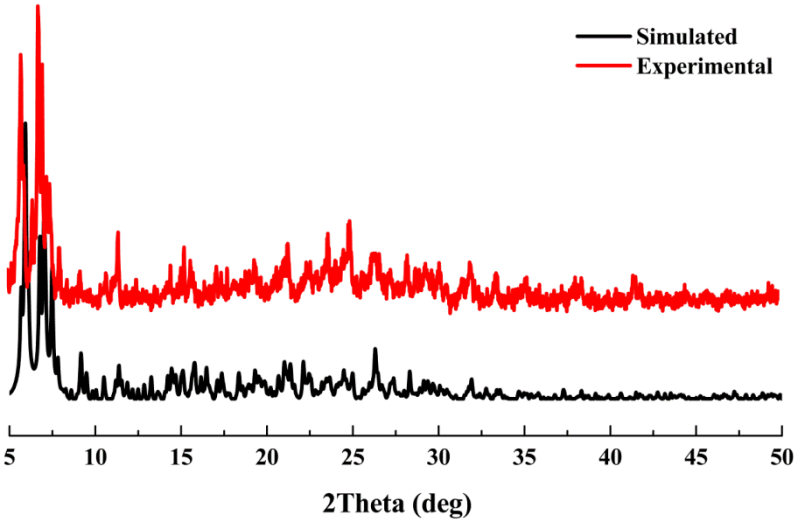

Fig. S2. The powder patterns of compound **PTC-95**.

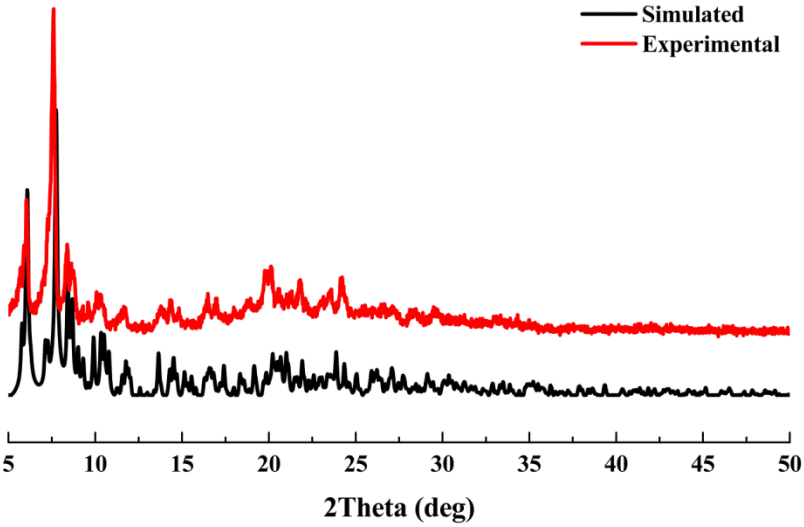

Fig. S3. The powder patterns of compound **PTC-96**.

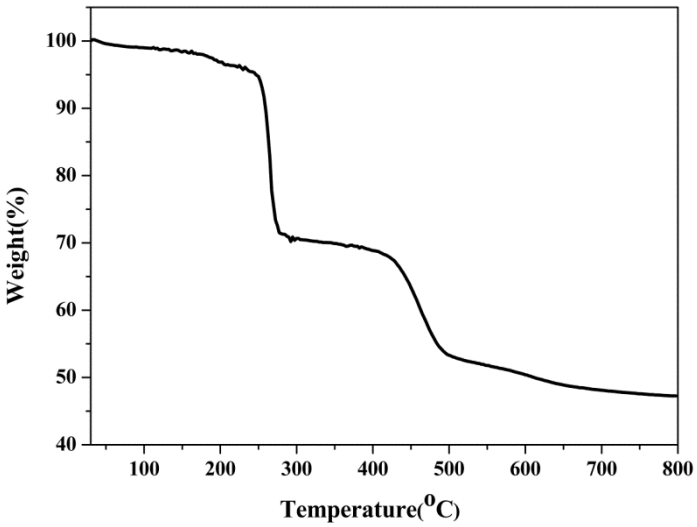

Fig. S4. TGA plots of **PTC-95**.

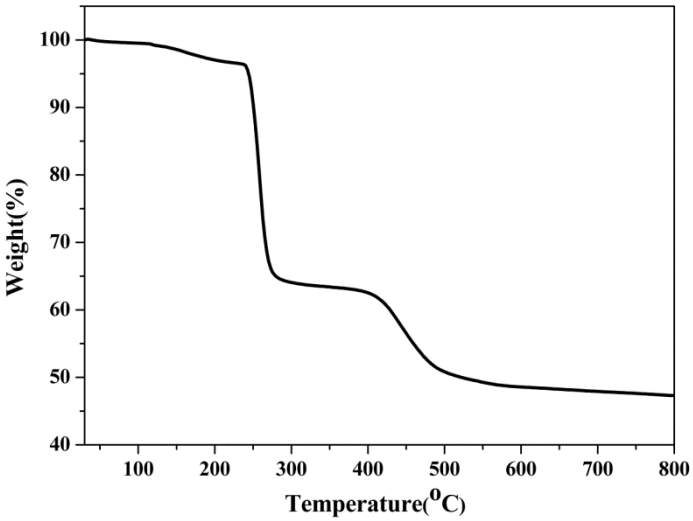

Fig. S5. TGA plots of **PTC-96**.

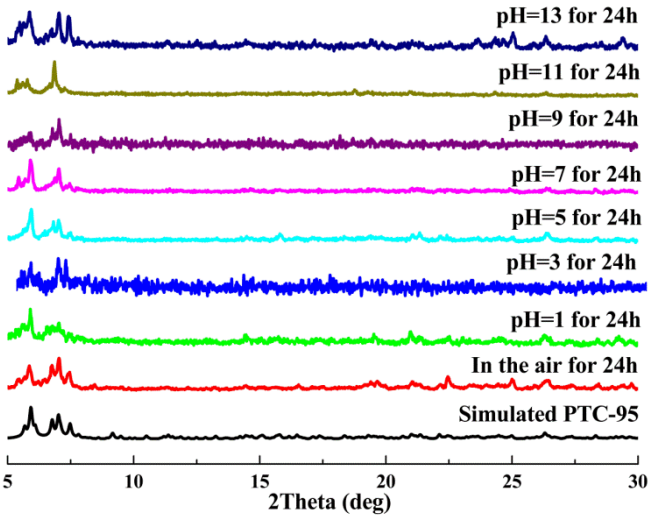

Fig. S6. Chemical stability tests of **PTC-95**.

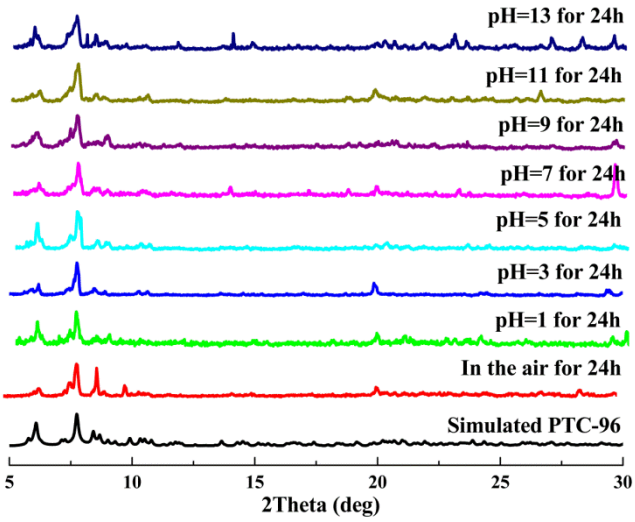

Fig. S7. Chemical stability tests of **PTC-96**.

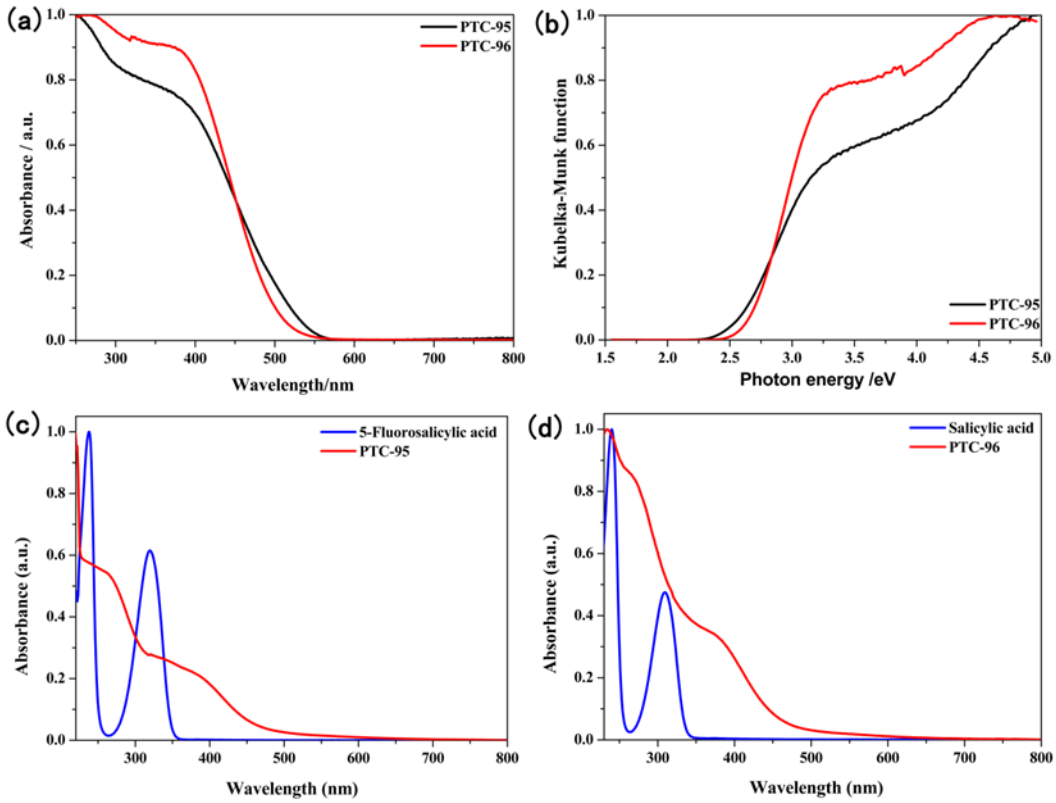

Fig. S8. (a) Solid-state UV-vis absorption spectra of **PTC-95** and **PTC-96**, respectively. (b) Kubelka–Munk transformation of diffuse reflectance data. (c) Solution UV-vis spectra of **PTC-95** and 5-fluorosalicylic acid in CH_2Cl_2. (d) Solution UV-vis spectra of **PTC-96** and salicylic acid in CH_2Cl_2.

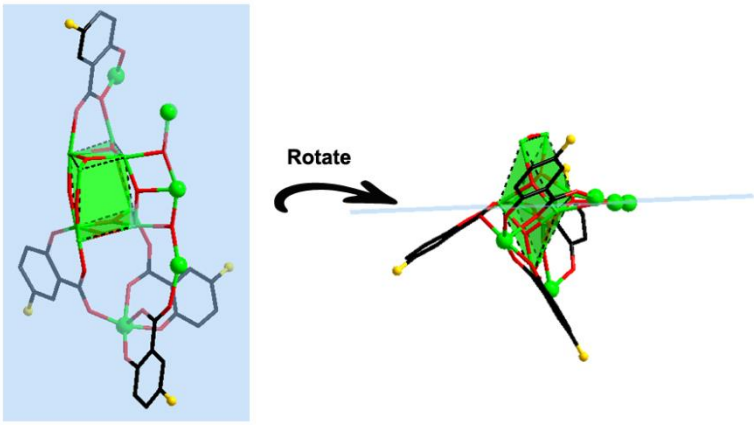

Fig. S9. The perspective view and side view of **PTC-95**.

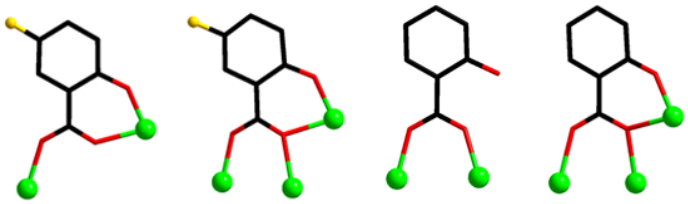

Fig. S10. Coordination modes of 5-fluorosalicylic acid and salicylic acid in **PTC-95** (μ_2-η^1:η^1:η^1; μ_3-η^1:η^2:η^1) and **PTC-96** (μ_2-η^1:η^1:η^0; μ_3-η^1:η^2:η^1).

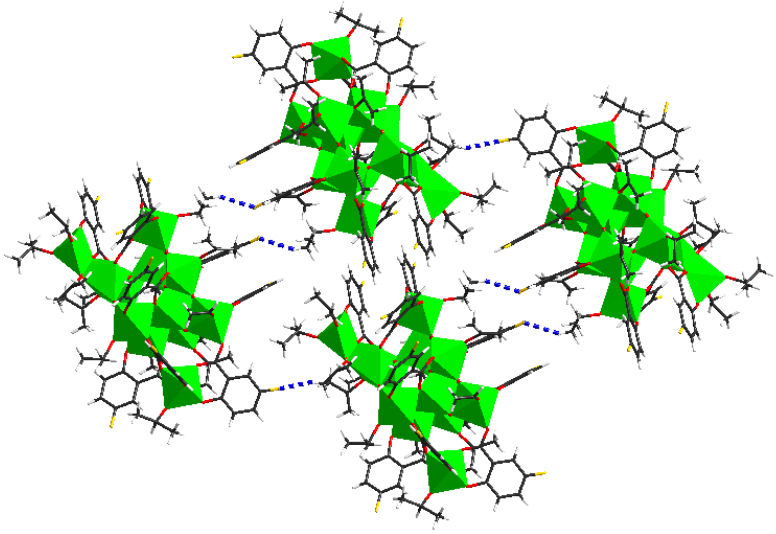

Fig. S11. Weak Hydrogen bonding interaction in **PTC-95**.

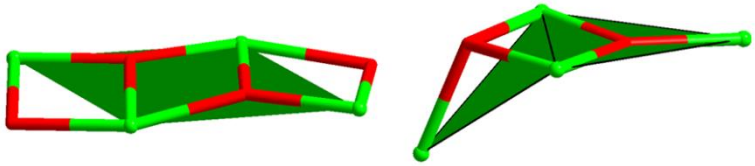

Fig. S12. Comparison of Ti_4 in **PTC-95** (left) and **PTC-96** (right).

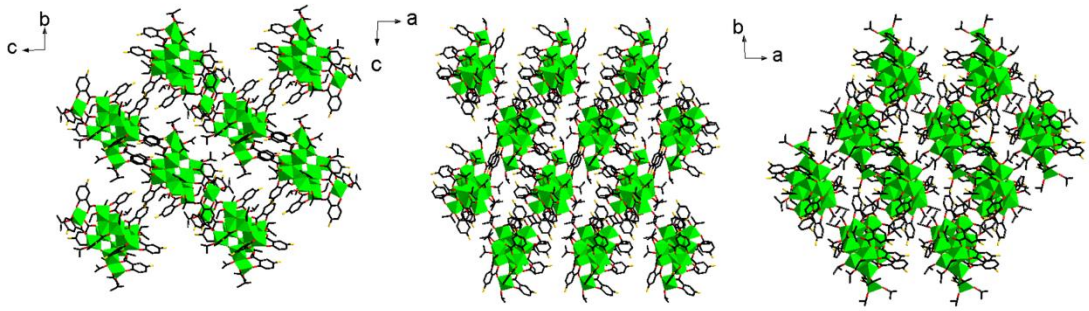

Fig. S13. The packing-view of **PTC-95** along with the [100], [010], and [001] direction.

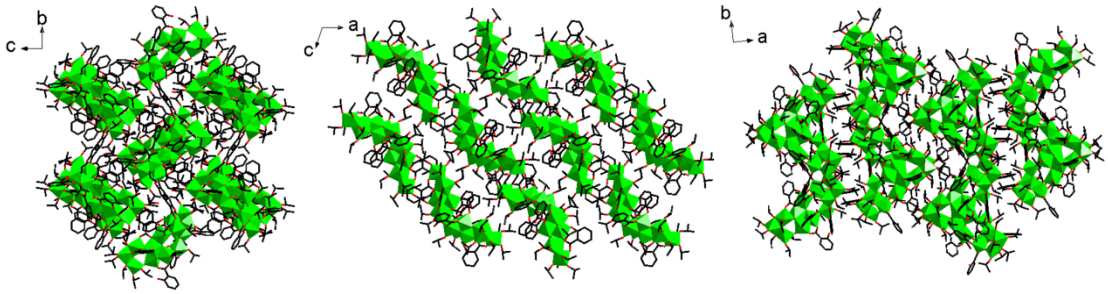

Fig. S14. The packing-view of **PTC-96** along with the [100], [010], and [001] direction.

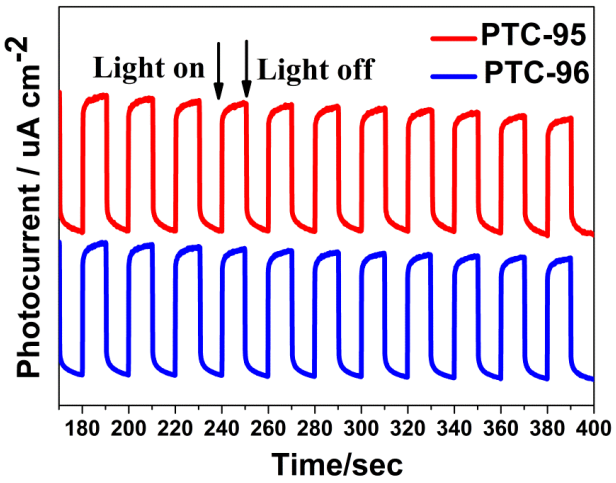

Fig.S15. Photocurrent responses of **PTC-95** and **PTC-96** in a 0.2 M Na_2SO_4 aqueous solution with 0.8 V (vs NHE) bias under full spectrum. The photocurrent densities were 0.2308 and 0.2275 $\mu A \cdot cm^{-2}$ for **PTC-95** and **PTC-96**, respectively.

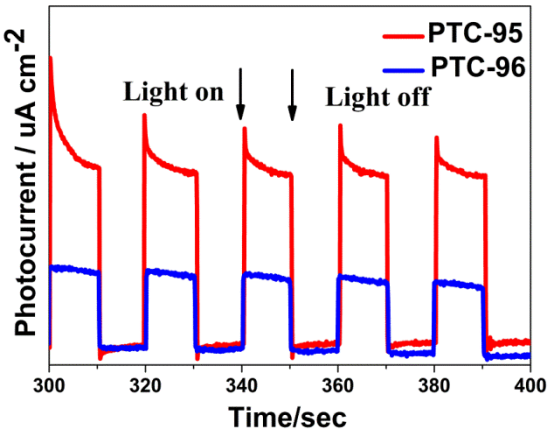

Fig.S16. Photocurrent responses of **PTC-95** and **PTC-96** in a 0.2 M Na_2SO_4 aqueous solution with 0 V (vs NHE) bias under repetitive visible light irradiate. The photocurrent densities were 0.0567and 0.0241 μA·cm^{-2} for **PTC-95** and **PTC-96**, respectively.

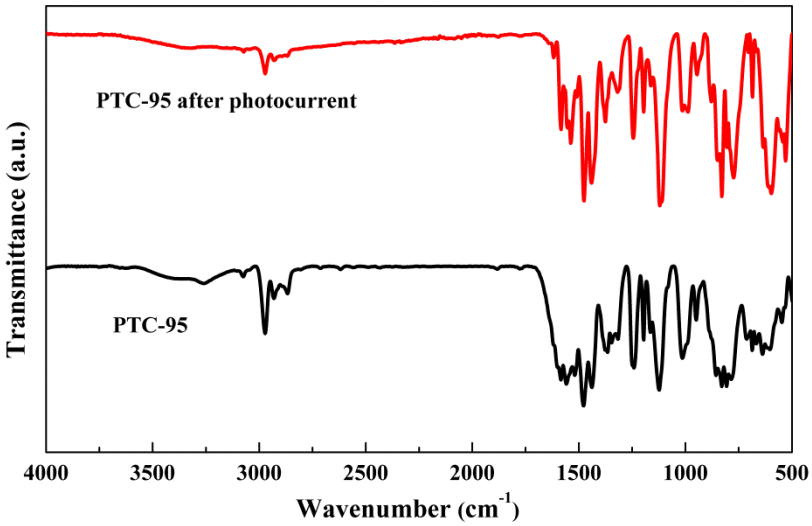

Fig. S17. Comparison of IR spectra of **PTC-95** before and after photocurrent test.

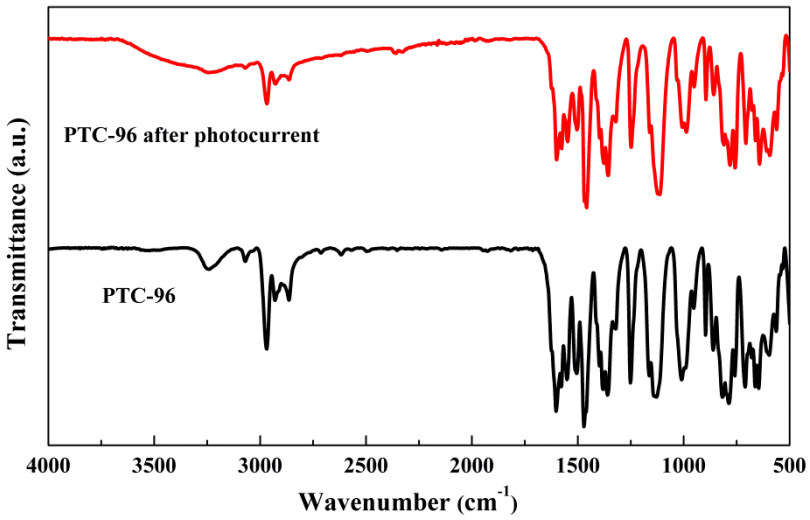

Fig. S18. Comparison of IR spectra of **PTC-96** before and after photocurrent test.

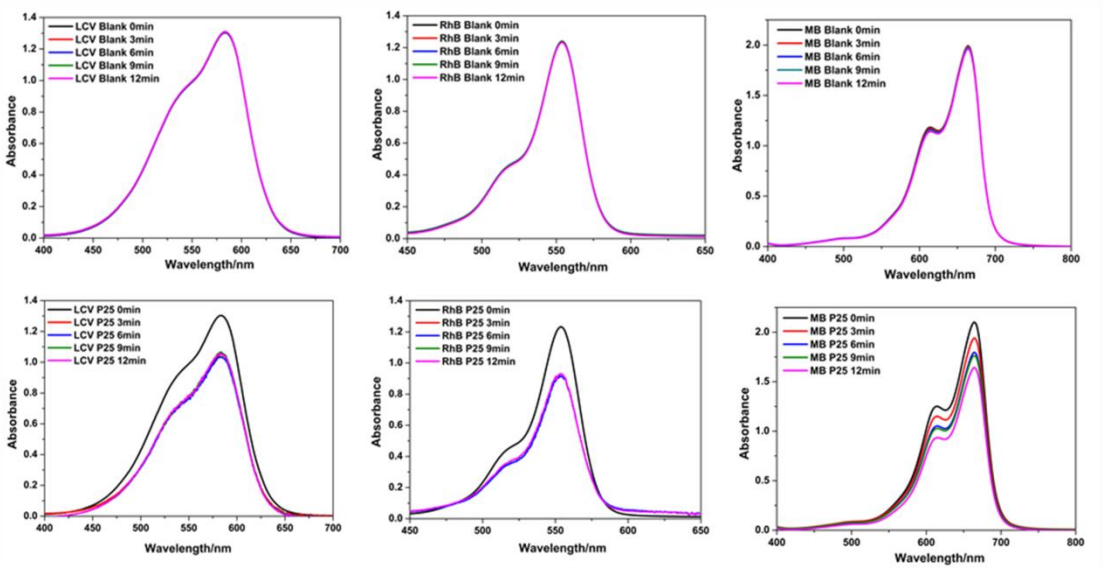

Fig. S19. The changes of UV–vis spectra of different dyes aqueous solutions (pH=7) on irradiation with visible light in blank (up) and in the presence of P25 (down).

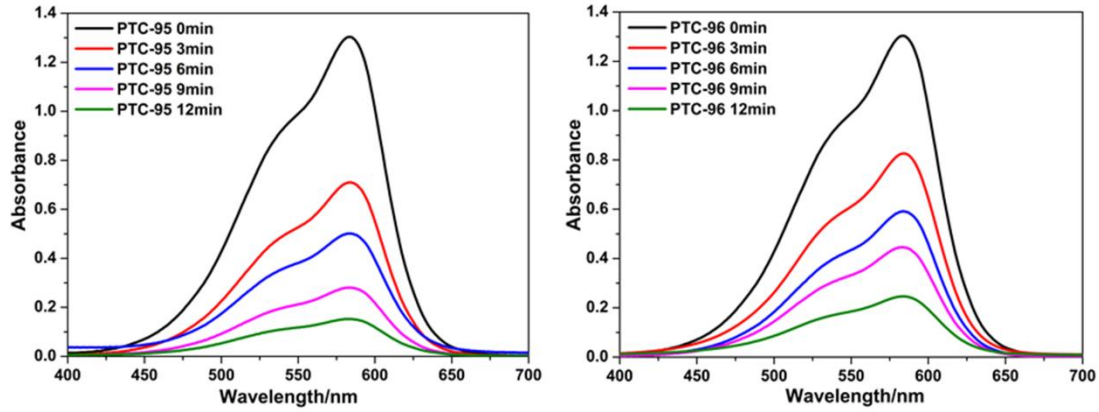

Fig. S20. The changes of UV–vis spectra of Leucocrystal Violet (LCV) aqueous solutions (30ppm) at pH=7 in the presence of PTC-95 and PTC-96, respectively.

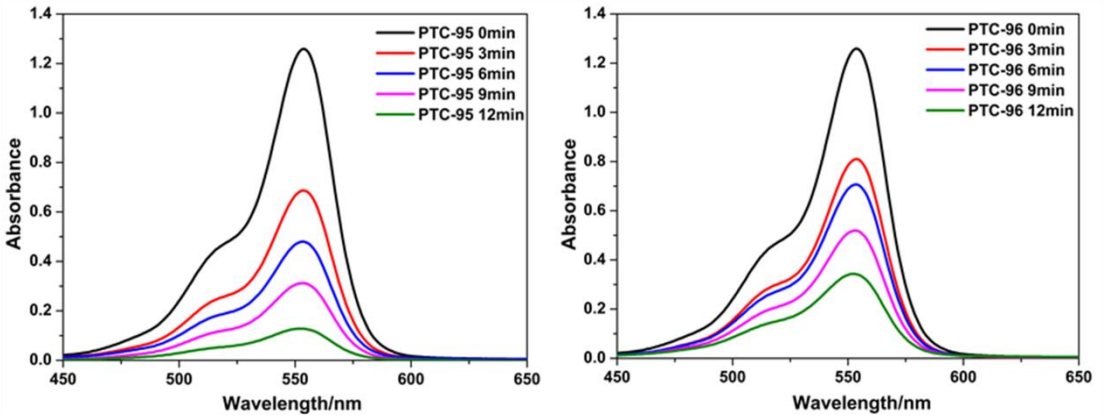

Fig. S21. The changes of UV–vis spectra of Rhodamine B (RhB) aqueous solutions (30ppm) at pH=7 in the presence of PTC-95 and PTC-96, respectively.

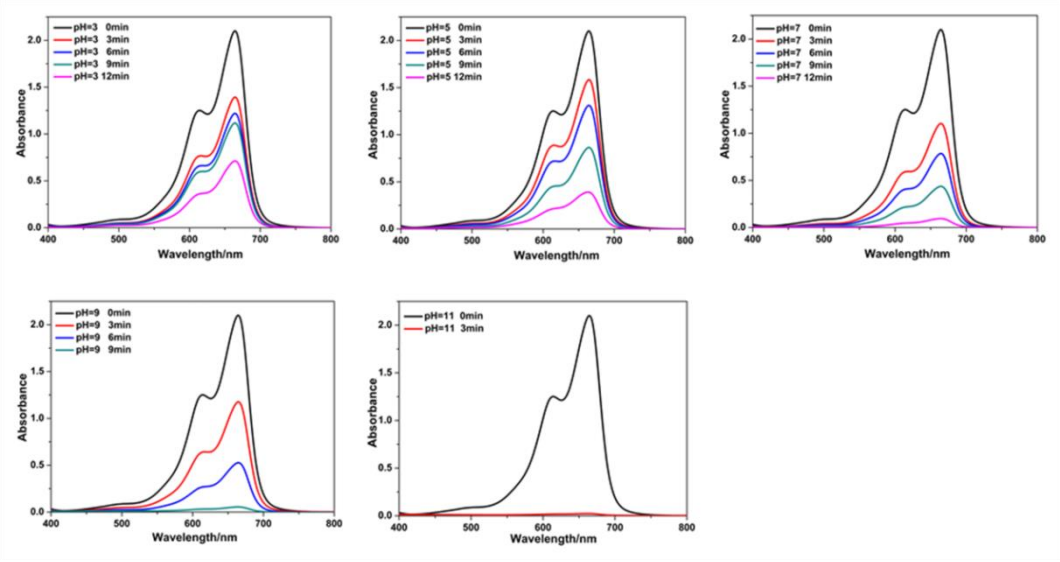

Fig. S22. The changes of UV–vis spectra of MB aqueous solutions at different pH in the presence of **PTC-95**.

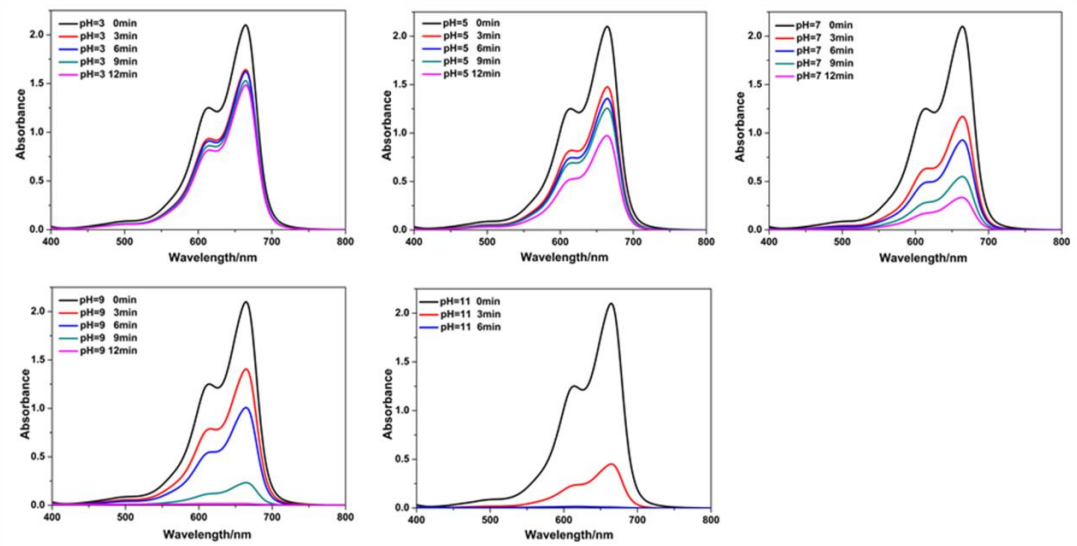

Fig. S23. The changes of UV–vis spectra of MB aqueous solutions at different pH in the presence of **PTC-96**.

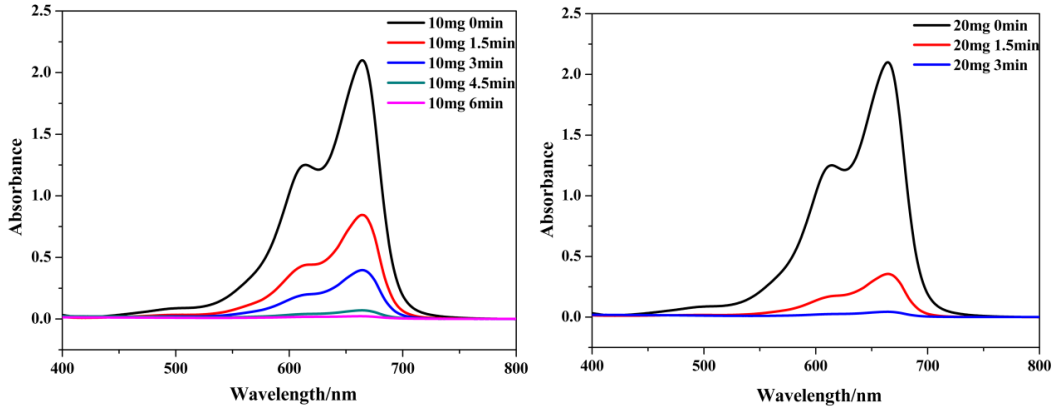

Fig. S24. The changes of UV–vis spectra of MB aqueous solutions (pH=11) with different quantities of **PTC-95**.

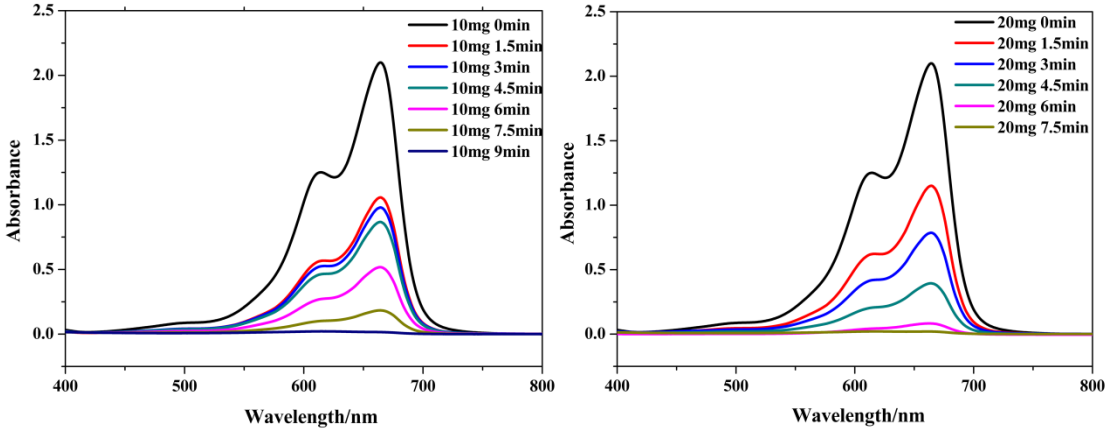

Fig. S25. The changes of UV–vis spectra of MB aqueous solutions (pH=11) with different quantities of **PTC-96**.

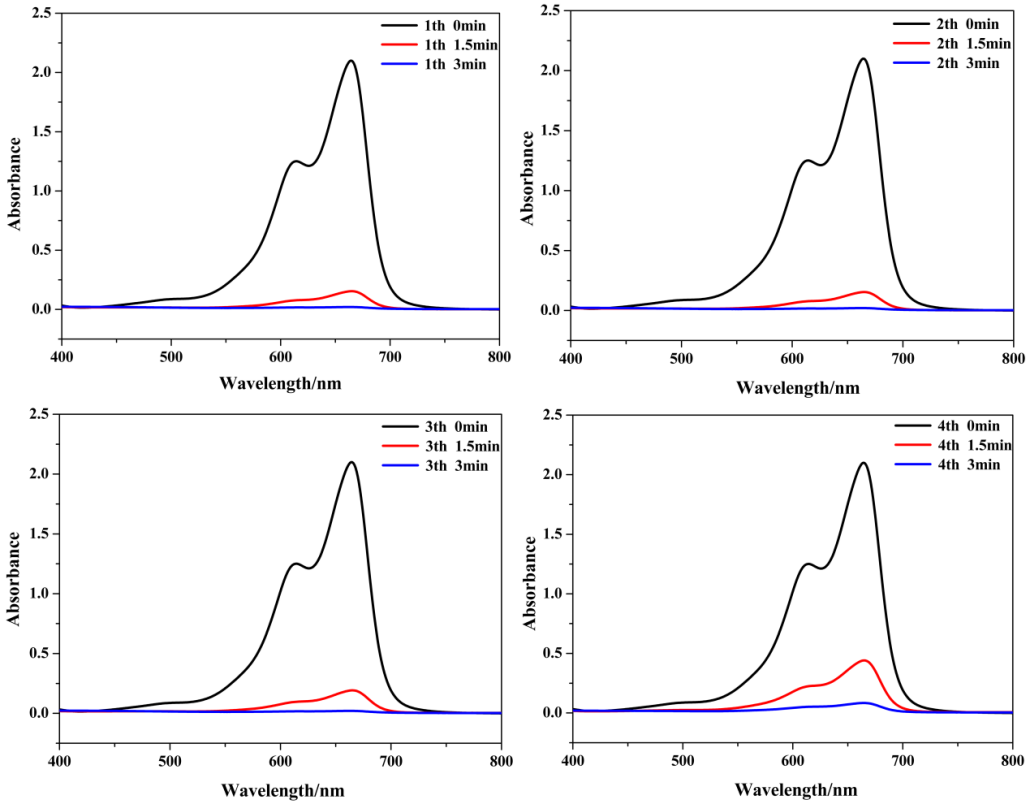

Fig. S26. Recycling tests of UV–vis spectra of MB aqueous solutions (pH=11) in the presence of **PTC-95**.

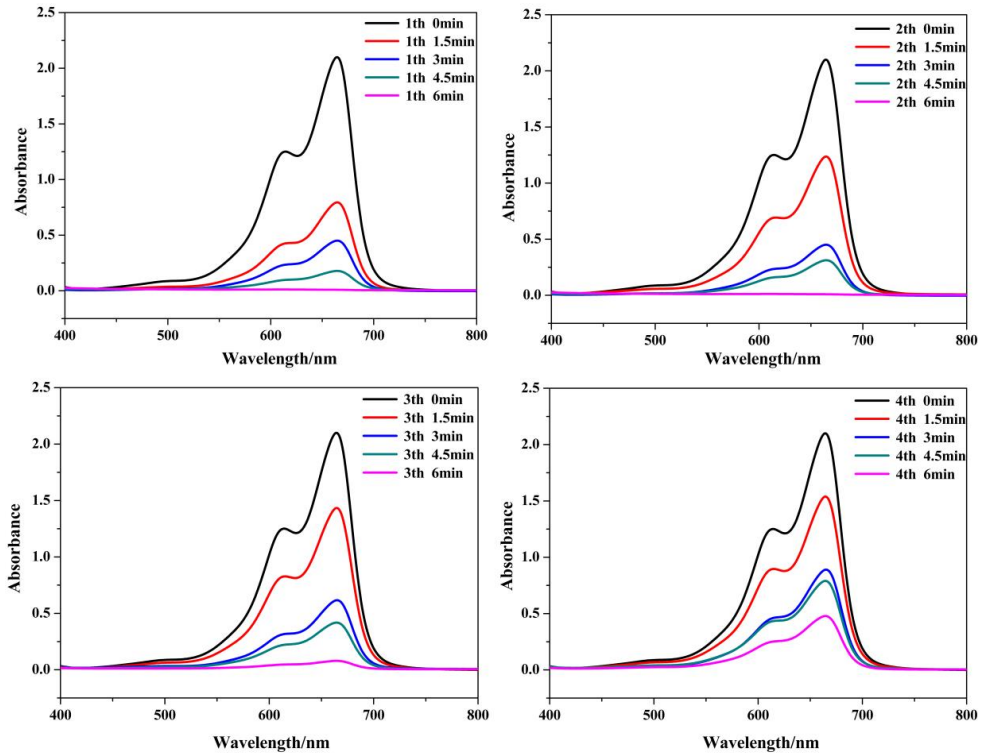

Fig. S27. Recycling tests of UV–vis spectra of MB aqueous solutions (pH=11) in the presence of **PTC-96**.

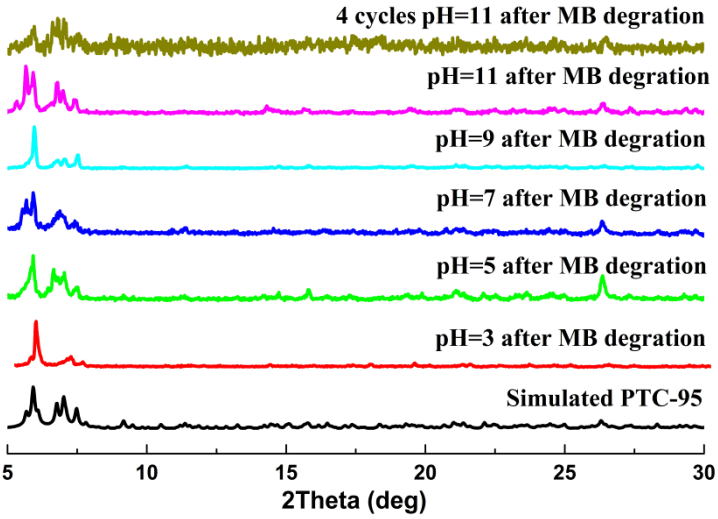

Fig. S28. The powder patterns of compound **PTC-95** after MB degradation.

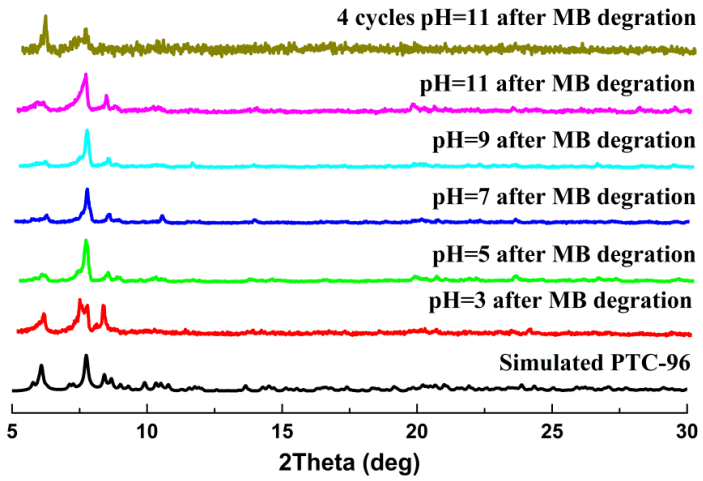

Fig. S29 The powder patterns of compound **PTC-96** after MB degradation.

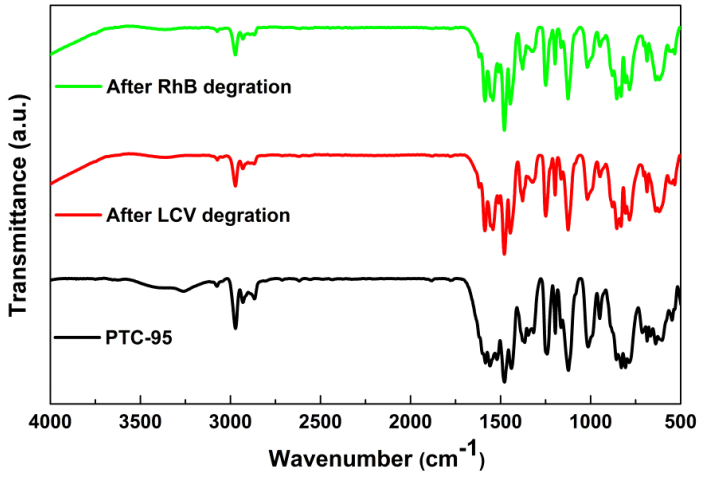

Fig. S30. Comparison of IR spectra of **PTC-95** before and after Leucocrystal Violet (LCV), Rhodamine B (RhB) degradation, respectively.

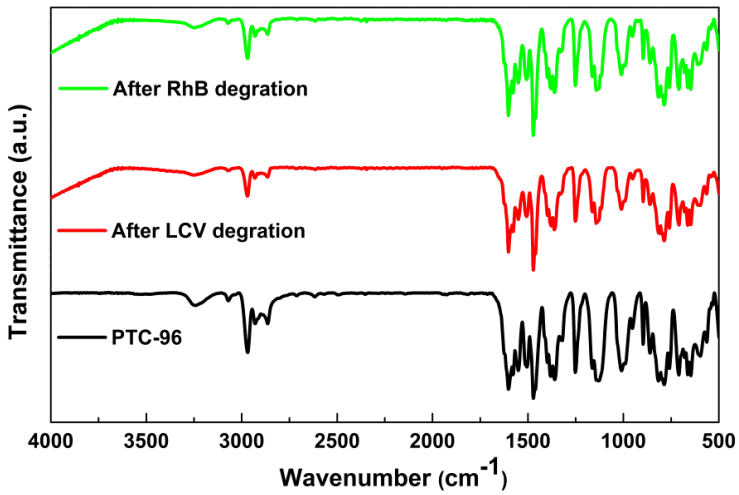

Fig. S31. Comparison of IR spectra of **PTC-96** before and after Leucocrystal Violet (LCV), Rhodamine B (RhB) degradation, respectively.

Table S1. Hydrogen bonds for **PTC-95** [Å and °].

D-H...A	d(D-H)	d(H...A)	d(D...A)	<(DHA)
C(034)-H(03D)...O(00T)#2	0.93	2.55	3.414(9)	154.5
C(03B)-H(03J)...O(01S)	0.93	2.55	3.352(10)	144.3
C(03U)-H(03V)...O(01P)	0.96	2.63	3.399(10)	137.6
C(045)-H(04M)...O(00U)	0.96	2.59	3.161(11)	118.1
C(04H)-H(05N)...F(01M)#3	0.96	2.57	3.204(12)	123.8
C(04I)-H(05Q)...F(01W)#4	0.96	2.53	3.418(12)	153.7
C(04R)-H(06J)...F(02B)#5	0.96	2.33	3.133(17)	140.5

Symmetry transformations used to generate equivalent atoms:

#1 -x+1,-y+2,-z+1; #2 -x+1,-y+1,-z; #3 -x,-y+1,-z; #4 -x+1,-y+2,-z; #5 x,y-1,z

Table S2. Hydrogen bonds for **PTC-96** [Å and °].

D-H...A	d(D-H)	d(H...A)	d(D...A)	<(DHA)
O(50)-H(50)...O(44)	0.82	1.90	2.587(5)	140.1
O(79)-H(79)...O(38)	0.82	1.88	2.599(6)	144.9
C(89)-H(89C)...O(4)	0.96	2.55	3.267(6)	131.8
C(105)-H(10C)...O(22)	0.96	2.53	3.232(6)	130.4
C(113)-H(11F)...O(24)	0.96	2.63	3.240(7)	121.8
C(130)-H(13C)...O(26)	0.96	2.50	3.235(7)	133.3
C(146)-H(14I)...O(48)	0.96	2.59	3.271(8)	128.4
O(104)-H(104)...O(17)	0.82	2.26	3.066(6)	167.0
C(3AA)-H(3AA)...O(81)	0.96	2.64	3.274(10)	123.6